CHEMISTRY OF MATERIALS

ARTICLE

pubs.acs.org/cm

Hydrothermal Stability of {001} Faceted Anatase TiO_2

Xiao Hua Yang,[†] Zhen Li,[‡] Chenghua Sun,[‡,§] Hua Gui Yang,*[,†] and Chunzhong Li*[,†]

[†]Key Laboratory for Ultrafine Materials of Ministry of Education, School of Materials Science and Engineering, East China University of Science & Technology, Shanghai, 200237, China,

[‡]ARC Centre of Excellence for Functional Nanomaterials and [§]Centre for Computational Molecular Science, Australian Institute of Bioengineering and Nanotechnology, The University of Queensland, Brisbane, Queensland 4072, Australia

Supporting Information

ABSTRACT: Due to its great importance in fundamental research and practical applications, tailored synthesis of anatase TiO_2 dominated with highly energetic {001} facets has been extensively studied during the past few years. However, clean (001) surface of anatase TiO_2 has been evidenced to be unstable and usually tends to reconstruct under ultrahigh-vacuum conditions. Thus, the stability of surface structure under other ambient conditions might be one of the most critical issues for anatase TiO_2 with exposed high-reactive {001} facets. In this study, the hydrothermal stability of {001} faceted anatase TiO_2 was systematically investigated by using single-crystalline anatase TiO_2 nanosheets with 80% {001} facets as a model starting material. Under hydrothermal conditions (200 °C in deionized water), anatase TiO_2 nanosheets can grow into larger single crystals with a truncated bipyramidal shape through an oriented attachment process along the [001] crystallographic direction, driven by the minimization of surface energy. Furthermore, the coarsening behavior and growth mechanism were discussed with the assistance of standard and high-resolution transmission electron microscopy, X-ray diffraction, X-ray photoelectron spectroscopy, and inductively coupled plasma optical emission spectrometry, as well as theoretical calculations. A modified kinetic model was also developed to elucidate the asymptotic growth of anatase TiO_2 nanosheets via oriented attachment mechanism. In addition, pH value and the solvents adopted during the treatments were revealed to have significant influence on the oriented attachment-based crystal growth due to suppression of hydrolysis of Ti−F groups on the surface. For example, the anatase TiO_2 nanosheets remained their original morphology unchanged when ethanol, propanol, butanol, or 1.5 M HCl aqueous solution was used as reaction medium.

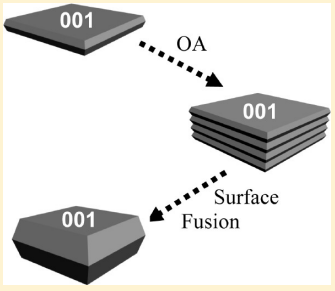

KEYWORDS: titanium dioxide, nanosheets, oriented attachment, hydrothermal stability, high-reactive facets

INTRODUCTION

Tailored synthesis of inorganic crystals with highly energetic/reactive surfaces has attracted great research interest over the past decades, due to their great importance in fundamental research and practical applications.[1−10] In particular, as one of the most important wide-band-gap semiconductors possessing unique chemical, electronic, and optical properties, anatase titanium dioxide (TiO_2) has been studied extensively because of its great potential applications in photovoltaic cells, photo/electrochromics, photocatalysis, photonic crystals, smart surface coatings, and sensors.[8−17] According to the principle of minimization of surface energy (0.90 J/m^2 for {001} > 0.53 J/m^2 for {100} > 0.44 J/m^2 for {101}), specific surfaces with high reactivity usually eliminate during the crystal growth process.[5,18−21] Under equilibrium conditions, natural and synthetic anatase TiO_2 single crystals mainly exist with a morphology of octahedral bipyramid, in which the majority of the surface is normally enclosed by energetically favorable {101} facets rather than the more reactive {001} facets.[5,7,22−24] Thus, it has been a great challenge to synthesize anatase TiO_2 with a large fraction of exposed {001} facets for a long time.

Recently, we synthesized high-quality anatase TiO_2 single crystals with 35−47% {001} facets for the first time by using HF as a capping agent under hydrothermal conditions.[10] After that, by use of similar synthetic strategies, {001} facet-dominated anatase TiO_2 crystals with various morphologies have been prepared and their superior performances in areas such as photocatalytic degradation of organic pollutants, solar-hydrogen production, and Li-ion batteries have been demonstrated as well.[25−34] With respect to fundamental research and practical applications of anatase TiO_2 dominated with highly reactive {001} facets, it would be desirable in most cases to remove the adsorbed species on the crystal surfaces. However, clean (001) surfaces of anatase TiO_2 were reported to be unstable and tend to reconstruct under ultrahigh-vacuum (UHV) conditions according to both theoretical and experimental results.[6,18,35−37] With the aid of low-energy electron diffraction (LEED), X-ray photoelectron spectroscopy (XPS), and angle-resolved mass spectroscopy of recoiled ions (AR-MSRI), Herman et al.[36] discovered the (1 × 4) reconstruction of anatase TiO_2 (001) surface and the subsequent formation of microfacets such as {103} and {$\bar{1}$03} facets with a lower surface energy than that of {001} facets, which indicates the low stability of the (001) surface of anatase TiO_2. Under UHV conditions, the

Received: March 28, 2011
Revised: June 21, 2011
Published: July 11, 2011

reconstructed surfaces are strongly stabilized, leading to the significant decrease of their reactivity.

Moreover, hydrothermal coarsening (i.e., Smoluchowski ripening) of anatase TiO_2 in aqueous solution have been extensively studied by Banfield and other researchers over the past decades.[38−41] It was found that when the aggregates of nanocrystalline TiO_2 particles coarsen under hydrothermal conditions, oriented attachment (OA) becomes an important crystal growth mechanism, which is quite different from the traditional Ostwald ripening (OR) process.[39a,40,41] Driven by surface energy reduction, adjacent anatase TiO_2 nanocrystals can self-organize spontaneously through sharing a common crystallographic orientation and then emerge together at a planar interface. Due to their unique two-dimensional (2D) shape, which can lead to easy stacking in a layer-by-layer mode, and the large amount of undercoordinated Ti_{5c} and functional groups on the clean (001) surface, anatase TiO_2 crystals with a 2D morphology might suffer significant structural re-forming, mainly caused by OA coarsening process. Unfortunately, the stability of anatase TiO_2 crystals dominated by high-reactive {001} facets under hydrothermal conditions has never been reported up to now.

In this work, we systematically investigated the hydrothermal stability of {001} faceted anatase TiO_2 nanosheets (NS) in an aqueous environment, and a plausible coarsening kinetic model was also developed. By monitoring the evolution of crystal structure and morphology of the TiO_2 NS during the hydrothermal treatment, it can be found that plane-to-plane crystal overlapping occurred and subsequently perfect lattice integrations along [001] crystallographic orientation took place, which is believed to be a typical OA process. Interestingly, the global single crystallinity of anatase TiO_2 was well-maintained after hydrothermal treatment. The findings in this work indicate that, under hydrothermal conditions, highly reactive {001} facets of the anatase TiO_2 NS tend to eliminate steadily via OA process along [001] crystallographic direction, which opens a pathway to a deeper understanding of their structural stability as well as the persistence of reaction in an aqueous environment.

EXPERIMENTAL METHODS AND THEORETICAL CALCULATIONS

Synthesis of {001} Faceted Anatase TiO_2. In this work, anatase TiO_2 NS with a high percentage of {001} facets was used as the starting material, which can be readily prepared through a simple hydrothermal method by using tetrabutyl titanate [$Ti(OBu)_4$, 98%, Aldrich] as Ti source and hydrofluoric acid (HF, 48%, Sigma−Aldrich) as capping agent.[26b,26c,28a] All of the chemicals were used as received without further purification. ***Caution:*** *Hydrofluoric acid (HF) is extremely corrosive and toxic and it should be handled with extreme care!* For a typical experiment, 5 mL of $Ti(OBu)_4$ and 0.6 mL of HF were added dropwise into a dried Teflon-lined stainless steel autoclave with a capacity of 50 mL. Then the autoclave was sealed and heated at 180 °C for 24 h in an electric oven. After completion of the reaction, the autoclave was taken out and cooled to room temperature. The product was collected by washing the precipitate thoroughly with absolute ethanol and deionized water for three times to remove the residual contamination. After drying at 80 °C in vacuum overnight, anatase TiO_2 NS dominated with {001} facets were finally harvested and then kept carefully for further characterization and the following experiments.

Hydrothermal Stability Study. Based on the as-prepared anatase TiO_2 NS with a large percentage of {001} facets, further hydrothermal treatments were performed in deionized water to investigate the stability of TiO_2 NS in aqueous environment. Typically, 15 mg of the as-synthesized dried TiO_2 NS was dispersed into 20 mL of deionized water under sonication, and subsequently the resulting mixture was carefully transferred to a Teflon-lined stainless steel autoclave with a capacity of 50 mL. Then the autoclave was sealed and heated at 200 °C for 88 h in an electric oven. Similar experiments were also carried out by altering the treatment time or replacing deionized water with other solvents such as ethanol, propanol, butanol, and 1.5 M HCl aqueous solution while keeping the other parameters unchanged. As a comparison, anatase TiO_2 single crystals with nearly 100% exposed {101} facets were also applied. The detailed synthetic method of the {101} faceted anatase TiO_2 single crystals has been described in our previous work.[26b] For all experiments, after the reaction, the clear supernatant in the reactor was taken out with a dropper and kept in a clean container for further characterization while the precipitate on the bottom was harvested by centrifugation and then rinsed thoroughly with deionized water.

Characterization. Powder X-ray diffraction (XRD) pattern was recorded on a Bruker D8 advanced X-ray powder diffractometer with Cu Kα radiation (λ = 1.5406 Å). The data was collected in the 2θ ranging from 10° to 80° with a scanning rate of 3°/min. Crystallographic morphology and lattice structure were observed by transmission electron microscopy, high-resolution transmission electron microscopy, and selected area electron diffraction (TEM/HRTEM/SAED, JEOL JEM2100) with an acceleration voltage of 200 kV. Chemical compositions as well as the surface bonding states of the samples were analyzed with X-ray photoelectron spectroscopy (XPS, Kratos Axis Ultra DLD). All binding energies were referenced to the C 1s peak (285.0 eV) arising from adventitious carbon. Prior to peak deconvolution, X-ray satellites and inelastic background (Shirley-type) were subtracted for all spectra. Moreover, the quantitative analysis of the surface species for each sample was determined by the fitted peak area. Concentration of Ti element in aqueous solution was analyzed by inductively coupled plasma optical emission spectrometry (ICP-OES, Thermo Elemental IRIS1000).

All TEM samples were prepared by depositing a drop of diluted suspension in ethanol on a copper grid. Samples for XRD and XPS analysis were prepared by drying the sedimented particles in vacuum overnight at 80 °C. Besides, liquid samples for ICP-OES analysis were obtained by centrifuging the supernatant in the Teflon container after reaction.The average particle size was derived statistically by using TEM images, and more than 50 particles were analyzed for each sample.

Theoretical Calculations. Spin-polarized density functional theory (DFT) calculations have been carried out with the DMol3 code.[42,43] The generalized gradient approximation (GGA) with the Perdew−Burke−Ernzerhof functional (PBE)[44] was utilized for all geometric optimization and single-point energy calculations. Effective core potentials with double-numeric quality basis and all electron potentials with double-numeric polarized basis have been employed for the description of core electrons during the optimization and the energy calculation, respectively. During our calculations, the convergence criteria for structure optimizations were set to (1) energy tolerance of 1.0×10^{-6} Ha/atom, (2) maximum force tolerance of 1.0×10^{-4} Ha/Å, and (3) maximum displacement tolerance of 1.0×10^{-3} Å. Monkhorst−Pack grid of 3 × 3 is used for the *k*-space sampling. Larger sets of *k* points were tested, making sure that there is no significant change in the calculated energies when a larger number of *k* points were used.

Also, (001) and (101) surfaces are modeled by 2 × 2 slabs with 12 atomic layers (four titanium layers), with a vacuum of 15 Å between neighboring slabs. During the geometric optimization, no atom is fixed, except that lattice parameters were fixed to experimental values. To investigate the coverage effect, three coverages, including $^1/_4$, $^1/_2$, and 1 monolayer (ML), have been investigated and fluorine-covered surfaces are also compared with clean ones. The relative stabilities of fluorine-terminated surfaces are indicated by the surface energies, which have been described in our previous publications.[10,25,27b]

dx.doi.org/10.1021/cm2008768 |*Chem. Mater.* 2011, 23, 3486–3494

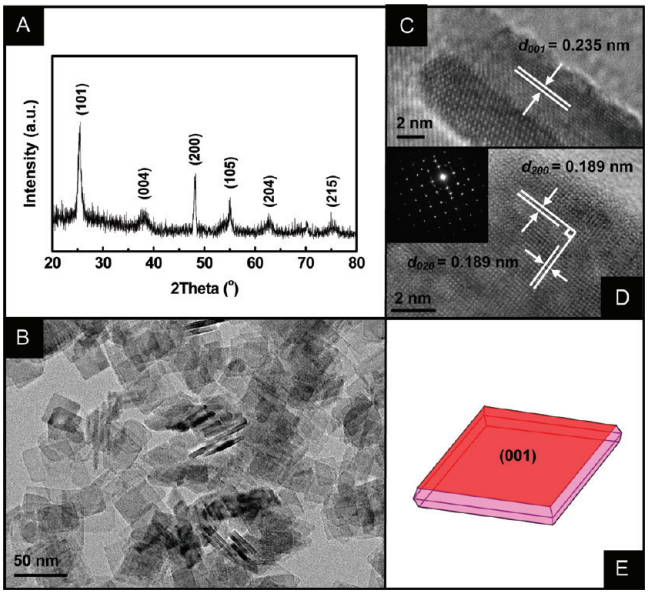

Figure 1. (A) Typical XRD pattern of the TiO_2 nanosheets synthesized by hydrothermal reaction of 5 mL of $Ti(OBu)_4$ and 0.6 mL of HF at 180 °C for 24 h. (B) Overview TEM image of the as-synthesized TiO_2 nanosheets. (C, D) HRTEM images of individual TiO_2 nanosheet recorded along [100]/[010] and [001] crystallographic directions, respectively, and (inset) corresponding SAED pattern. (E) Morphological model of a single {001} faceted TiO_2 nanosheet.

RESULTS AND DISCUSSION

To investigate the stability of {001} facets of anatase TiO_2, it is essential to prepare anatase TiO_2 sample with a high percentage of {001} facets. Our approach in this work is based on the one-pot hydrothermal synthesis of anatase TiO_2 NS with approximately 80% {001} facets.[26b,26c,28a] XRD and TEM were employed to confirm the crystal structure and morphology of the as-prepared TiO_2 sample. Figure 1A shows the typical XRD pattern of the resulting product, and the diffraction peaks with $2\theta = 25.3°$, 37.8°, and 48.1° can be indexed to (101), (004), and (200) crystal planes of anatase TiO_2 (tetragonal, $I4_1/amd$, JCPDS 21-1272), respectively, indicating its pure anatase TiO_2 phase. Figure 1B presents the TEM image of the product, which reveals that the obtained TiO_2 product consists of uniform, well-defined sheet-shaped structures possessing a rectangular outline. Statistically, the anatase TiO_2 NS have a side length of 50 nm and a thickness of 5 nm on the average. HRTEM images of the anatase TiO_2 NS viewed along [100]/[010] and [001] crystallographic directions (Figure 1C,D), as well as the SAED pattern (inset, Figure 1D) further confirm that the square surfaces are {001} facets of the single-crystalline anatase TiO_2 NS. The corresponding schematic illustration of a free-standing anatase TiO_2 nanosheet is presented in Figure 1E, in which the top and bottom surfaces stand for the dominant {001} facets and the other surfaces represent the thermodynamically stable {101} facets. Because the angle between neighboring (001) and (101) surfaces is 68.3°,[10,26e] and the average side length and thickness is 50 and 5 nm, the percentage of exposed {001} facets can be calculated to be ~80%. On the basis of this structural information, it can be concluded that anatase TiO_2 NS with dominant {001} facets has been readily prepared and can be used for the following stability experiments.

In the present work, the hydrothermal stability of {001} faceted anatase TiO_2 in an aqueous environment was examined

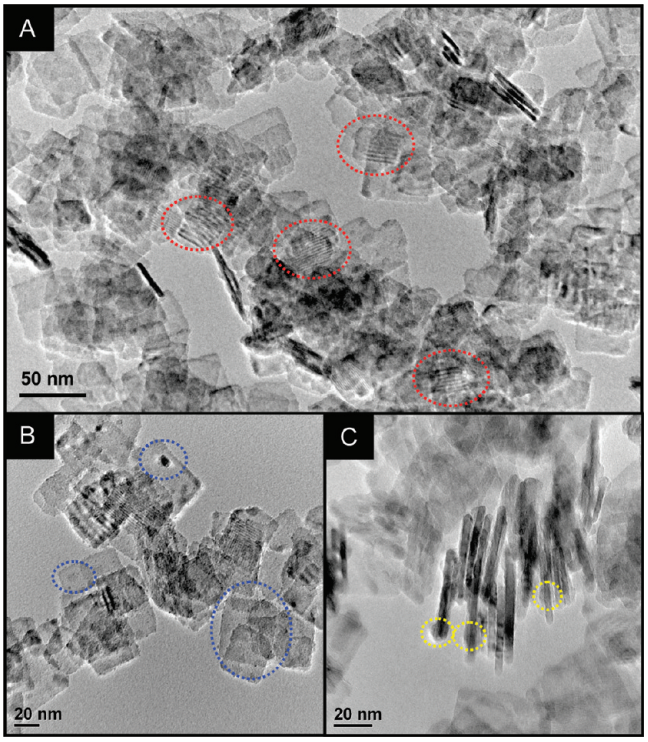

Figure 2. (A) Low- and (B, C) high-magnification TEM images of the product prepared by hydrothermal treatment of as-synthesized TiO_2 nanosheets in deionized water at 200 °C with a reaction time of 105 min. The areas marked by red dotted circles in panel A indicate the Moiré patterns frequently observed in the TEM images. The areas marked by blue dotted circles in panel B and yellow dotted circles in panel C present the irregular "nonflat" surfaces of the resulting product and the small particles attached on the adjacent nanosheets, respectively.

by dispersing 15 mg of as-synthesized TiO_2 NS in deionized water and then treating the suspension at 200 °C for a specific time. Figure 2 illustrates representive TEM images of the product with a reaction time of 105 min. From the low-magnification TEM image shown in Figure 2A, it can be observed that most of the anatase TiO_2 NS still have a sheetlike shape with a thickness of 4−6 nm and a side length of 30−60 nm. On the whole, the crystal size and morphology of the anatase TiO_2 NS on current stage have no significant change compared to the starting material. However, according to the high-magnification TEM images (Figure 2B,C), it can be concluded that (001) surfaces of the TiO_2 NS after hydrothermal treatment became rough with some small particles attached, as indicated by the circles with dashed lines in Figure 2B,C. These phenomena can be considered as results of surface hydrolysis and subsequent partial dissolution of the starting anatase TiO_2 NS. For monodisperse anatase TiO_2 NS, Ti atoms on the surface can dissolve into the reaction medium and finally lead to rough surface. Meanwhile, the Ti-containing complex formed by dissolving the original TiO_2 crystals may nucleate homogeneously on the high-energy (001) surface of existing anatase TiO_2 NS. Herein, ICP-OES was performed to examine the concentration of Ti-containing species in the solution after hydrothermal reaction. The relative mass concentration of Ti element in the aqueous solution was 7.8×10^{-4}. That is, around 0.5% of the original solid anatase TiO_2 NS was dissolved into water during the hydrothermal treatment,

dx.doi.org/10.1021/cm2008768 |Chem. Mater. 2011, 23, 3486–3494

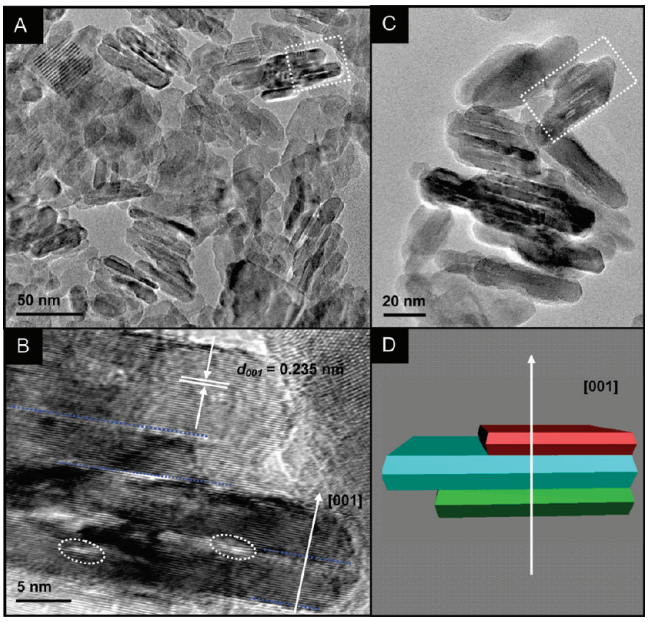

Figure 3. (A) Low-magnification TEM image and (B) corresponding HRTEM image of the sample prepared by hydrothermal treatment of as-synthesized TiO_2 nanosheets in deionized water at 200 °C with a reaction time of 200 min. (C) Typical TEM image of larger intermediates frequently observed in the product. (D) Schematic model of oriented attachment of {001} faceted anatase TiO_2 nanosheets. Blue dotted lines in panel B represent boundaries between individual nanosheets; areas marked with white dotted circles show the holes/gaps within larger particles composed of nanosheets.

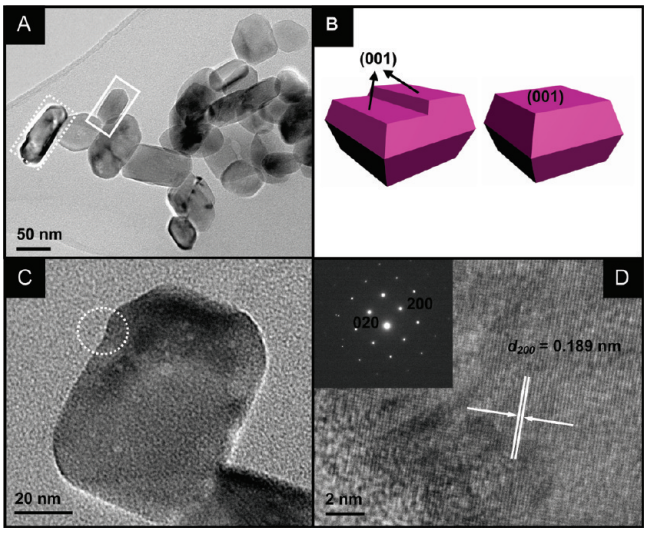

Figure 4. (A) TEM image of the product derived from hydrothermal treatment of TiO_2 nanosheets in deionized water at 200 °C for 88 h. Areas enclosed by dotted and solid lines denote representative particles with flat and stepped surfaces, separately. (B) Corresponding morphological models of the marked particles shown in panel A. (C) TEM image of an individual particle. (D) HRTEM image and (inset) SAED pattern recorded in the circled area in panel C.

which was determined by solid−liquid equilibria principles and thus led to the slight morphology/size changes.

Interestingly, many Moiré patterns can be observed on the stacked anatase TiO_2 NS, as shown in Figure 2A. This phenomenon was due to interference between the crystalline lattices of the stacked anatase TiO_2 NS, as reported by Weller and co-workers[45] during the synthesis of PbS sheets via OA. The stacking of anatase TiO_2 NS increases the possibility of OA, which resulted in the elimination of {001} facets. OA has been experimentally proved to be one of the most important mechanisms for crystal coarsening under hydrothermal conditions. During the process, adjacent particles often organized spontaneously with common crystallographic orientation. In the present study, due to the similar structural features and surface properties of anatase TiO_2 NS, stacking of NS decorated by small dots along [001] crystallographic direction can be frequently observed in the TEM images (see Figure 2B,C).

Figure 3 shows the TEM images of the product derived from hydrothermal treatment of the anatase TiO_2 NS in deionized water for a longer time. As the reaction time extended to 200 min, the original shape of anatase TiO_2 NS can hardly be identified, as shown in Figure 3A,C. Secondary particles formed and most of them were generated by OA of 2−8 original anatase TiO_2 NS, which can still be judged. Arrows in Figure 3B indicate that all the anatase TiO_2 NS building blocks self-assemble along the same crystallographic direction. The interplanar crystal spacing of 0.235 nm demonstrates the OA of anatase TiO_2 NS along the [001] crystallographic direction. Figure 3D schematically shows the OA-based assembly process. It should be noted that, on the current stage, many tiny holes and narrow gaps exist between the individual anatase TiO_2 NS, as shown in Figure 3B, which is caused by the OA of TiO_2 NS with nonflat rough surfaces and can be eliminated through further crystal growth. Even though twins, stacking faults, and misorientation are usually involved during the OA process,[39a,40a] primary building units do have the capability of rotation alignment to get structurally consistent secondary anatase TiO_2 crystals.

When anatase TiO_2 NS were heat-treated in deionized water for 88 h, large anatase TiO_2 single crystals can be synthesized with sizes ranging from 50 to 100 nm, as shown in the TEM image in Figure 4A. According to the morphology evolution on different stages, the current product should possess a truncated bipyramidal shape with lower percentage of {001} facets. Moreover, most of the anatase TiO_2 crystals on the current stage exhibit smooth flat surfaces and only a few crystals have a stepped surface, which are highlighted by solid and dotted lines, respectively, in Figure 4A. Accordingly, Figure 4B gives structural models of these two typical single crystals. According to the proposed OA-based formation mechanism, anatase TiO_2 crystals with a stepped surface were generated by the OA of TiO_2 NS with a different lateral size. Figure 4C shows the TEM image of a typical anatase TiO_2 crystal, and the corresponding HRTEM/SAED results are provided in Figure 4D. The SAED pattern indicates the single-crystalline characteristic of the as-obtained anatase TiO_2 particles, and the HRTEM image clearly demonstrates atomic planes of (200) or (020) crystal faces with *d*-spacing of 0.189 nm and an interfacial angle of 90°. On the basis of this structural information, the top and bottom surfaces of the truncated bipyramid can be assigned to highly reactive {001} facets of anatase TiO_2. Furthermore, the average crystal size along the [001] direction was statistically estimated to be 28.3 nm, which is about 6 times the thickness of the original {001} faceted TiO_2 NS. However, the side length of the product on the current stage is 67.5 nm on average, which is quite close to that of the starting anatase NS, providing strong evidence for the

dx.doi.org/10.1021/cm2008768 |*Chem. Mater.* 2011, 23, 3486–3494

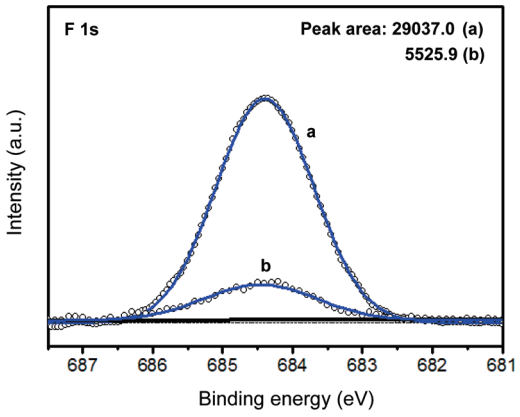

Figure 5. High-resolution XPS spectra of F adsorbed on the surfaces of anatase TiO_2 nanosheets (a) before and (b) after hydrothermal treatment in deionized water at 200 °C for 88 h. (○) Raw data; black and blue lines represent base and fitted lines, respectively.

OA-based crystal growth mechanism. Therefore, the percentage of {001} facets of anatase TiO_2 crystals was calculated to be 45.6% on this stage.

By monitoring the morphology evolution of anatase TiO_2 NS within 88 h under hydrothermal conditions, it can be concluded that {001} faceted TiO_2 NS is unstable and can eventually develop into TiO_2 crystals with a lower percentage of {001} facets in deionized water. Furthermore, as indicated in Figure S1 (Supporting Information), if the time of hydrothermal treatment was extended as long as 120 h, it can be found that the final product shows a round shape, which may illustrate more {101} facets formed.

Because the absorbates on the crystal surface can change the surface energy and also have the capability to alter the OA mode between the primary nanoparticles, XPS was applied to analyze the surface species and bonding states. Figure S2 panels A and B (Supporting Information) show the wide-scan XPS survey spectra of the starting anatase TiO_2 NS and the corresponding product synthesized through hydrothermal treatment for 88 h, respectively. Obviously, wide-scan XPS spectra of the two samples possess a similar pattern on the whole. The oxidation state of the Ti element (Ti 2p3/2, binding energy 458.8 eV; Ti 2p1/2, binding energy 464.3 eV) can be assigned to that of bulk TiO_2, as reported previously.[10] Figure 5 shows the high-resolution XPS spectra of F element existing on the surface of the initial anatase TiO_2 NS and the final product after hydrothermal treatment, where the binding energy was measured to be 684.5 eV, corresponding to the typical value for the surface Ti−F species.[46] Judging from the calculated peak areas, it can be revealed that the relative F content adsorbed on the surface decreased remarkably, and nearly 67% of the original F element adsorbed on the surface was removed after hydrothermal reaction.

Under equilibrium conditions, the shape of a crystal is generally determined by the principle of minimization of the total surface free energy under the constraint of fixed volume.[22] Stability of the facets (or the growth rate in different crystal orientations) often results in a shape that is uniquely defined by the nature and concentration of the adsorbates.[45] On the basis of the XPS analysis and morphology evolution discussed above, it can be summarized that the concentration of F ions adsorbed on the TiO_2 surface plays a major role in shape controlling for the final product and the percentage of {001} facets as well. Through theoretical calculation of the surface energy, the percentage of {001} facets was estimated as a function of the F coverage (θ) on the anatase TiO_2 surface. The calculated data and corresponding diagram are presented in Table 1 and Figure 6 respectively. In addition, the insets in Figure 6 provide the thermodynamic models for anatase TiO_2 single crystals with different percentages of {001} facets. It is worth noting that the corner effect resulting from the cross part of two surfaces was not considered in the calculation. For anatase TiO_2 NS with 80% {001} facets, the corresponding θ was estimated to be 0.45. Thus, according to the relative F concentration in XPS results, the F coverage for the sample treated in deionized water can be calculated to be about 0.1 and the derived percentage of {001} facets should be around 0.4% only. This value indicates the trend of the elimination of the {001} facets, which is consistent with the TEM observations in Figures 2−4.

Table 1. Calculated Energies of (001) and (101) Surfaces and Corresponding S_{001}/S_{total} as a Function of F Coverage (θ) for Anatase TiO_2 Single Crystals Exposed Only with {001} and {101} Facets

θ	γ_{001} (J·m^{-2})	γ_{101} (J·m^{-2})	S_{001}/S_{total} (%)
0	0.96	0.41	0.3
0.25	0.44	0.20	0.5
0.50	−0.03	0.00	100
1	−0.71	−0.39	100

In addition to the changes of crystal morphology after hydrothermal treatment, the size alteration along one specific crystal growth direction is also helpful to understand the kinetics. Figure 7 presents XRD patterns of anatase TiO_2 products after different hydrothermal treatment time. When the anatase TiO_2 NS were treated in deionized water for a reaction time ranging from 60 min to 88 h, all of the diffraction peaks match well with the crystal structure of the anatase TiO_2 phase and no other phases can be detected. Nevertheless, diffraction peaks of the samples became stronger and sharper with increasing reaction time, especially for the diffraction peaks at $2\theta = 37.80°$ corresponding to (004) planes of anatase TiO_2, which suggests oriented growth of anatase TiO_2 NS along the [001] direction. By use of the Scherrer equation, crystal dimensions in the [001] direction are determined to be 16.5, 16.5, and 44 nm for the TiO_2 samples shown in Figures 2, 3, and 4, respectively. The calculated sizes of the products at these early stages does not match well with the values derived from TEM images, which might be attributed to some close stacking of the anatase TiO_2 NS in the [001] direction.

To investigate the crystal growth kinetics of anatase TiO_2 NS in an aqueous environment, systematic hydrothermal experiments with different reaction time were carried out. Figure S1 (Supporting Information) shows TEM images of the resulting products with reaction time of 1, 6, 11, 48, and 120 h. By comparison with the starting anatase TiO_2 NS, it can be concluded that the shape and size of the products changed insignificantly in the early stages of hydrothermal treatment. With increasing reaction time, monodisperse anatase TiO_2 NS was eliminated steadily and larger aggregates of TiO_2 NS appeared within the initial stages of hydrothermal treatment. According to detailed analysis of the sample in this critical period, the larger particles have been evidenced to form via OA of the

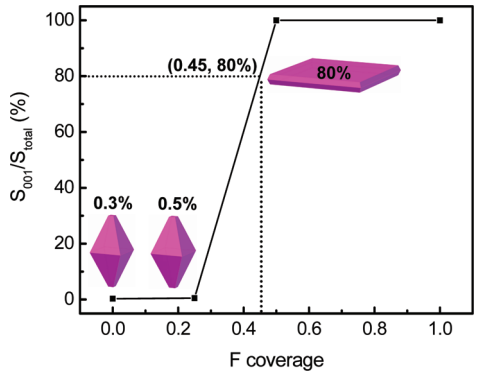

Figure 6. Relationship between calculated S_{001}/S_{total} and F coverage of the single-crystalline anatase TiO_2 crystals enclosed by low-index {001} and {101} facets. (Insets) Corresponding thermodynamic models for anatase TiO_2 with 0.3%, 0.5%, and 80% exposed {001} facets, respectively.

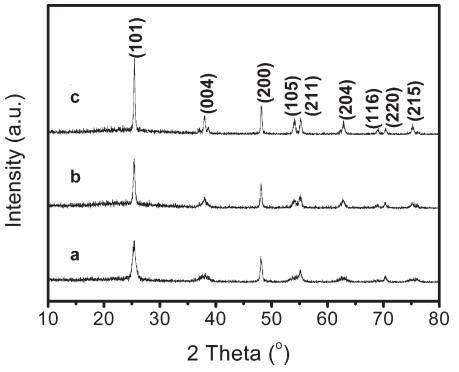

Figure 7. XRD patterns of the samples derived from hydrothermal treatment of TiO_2 nanosheets in deionized water at 200 °C for (a) 105 min, (b) 200 min, and (c) 88 h.

original anatase TiO_2 NS as building blocks along the [001] crystallographic direction. With reaction time further prolonged, the large particles became smooth and well-faceted along with a significant increase in size, especially for the crystal dimension in [001] orientation. Therefore, OA-based crystal growth played a leading role in the crystal coarsening that occurred during hydrothermal treatment of anatase TiO_2 NS in deionized water.

In general, the kinetics of crystal growth and coarsening are mainly determined by the nature of the interface between primary crystals and the surrounding solution, the format of metal-containing species in the solution, and the structure of the crystals.[39a,40,41] For OA-based crystal growth of {001} faceted anatase TiO_2 NS, perfect OA involves spontaneous self-organization of adjacent TiO_2 NS, which makes them share a common [001] crystallographic orientation, removal of the adsorbed capping agents such as F, and formation of the new chemical bonds at the interface between primary crystals. Bonding between the original anatase TiO_2 NS can reduce overall surface free energy through complete elimination of the crystal−liquid interface. As a result, the secondary anatase TiO_2 crystals are new single crystals composed of oriented subunits. In the present work, a kinetic model is proposed to elucidate the crystal growth process of {001} faceted anatase TiO_2 NS via OA mechanism during the hydrothermal reaction, which have been confirmed

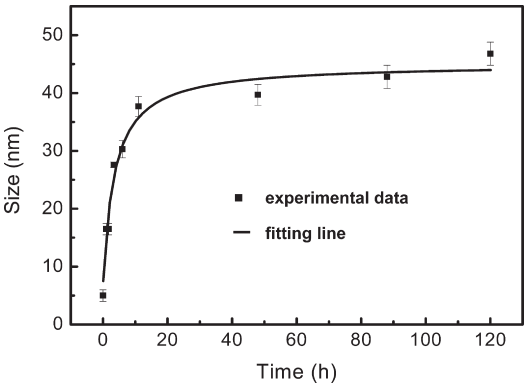

Figure 8. Experimental data and simulation result showing the increase of particle size along the [001] crystallographic direction vs treatment time. The average particle size of the samples with different reaction time was calculated from the XRD pattern shown in Figure S3 (Supporting Information) by use of the Scherrer equation.

through TEM/HRTEM analysis of typical samples with different reaction time. Moreover, the thickness of the products multiplied in a short time while the side length of the products was nearly unchanged during the process. Herein, the average crystal size in the [001] direction and the number of initial particles were supposed to be H_0 and N_0 at $t = 0$, respectively. After growth via OA for a period of time t, the number of primary particles is $N(t)$, and the average particle size along the [001] direction of newly generated particles is H, separately. It should be noted in this kinetic model that the TiO_2 crystals were supposed to be rectangular if viewed through the [001] zone axis, and the side length was unchanged during crystal growth.

On the basis of the general kinetic model applied for OA-based crystal growth,[47,48] the proposed kinetic equation in this work was simulated to be

$$H = \frac{H_0(nk_1t + 1)}{(k_1t + 1)} \quad (1)$$

In this formula, $k_1 = kN_0$, and n is a constant representing the average number of building blocks composing a single particle. According to the average crystal size along the [001] direction of the starting material and the final product, n was assumed to be 6. In this case, eq 1 changes to

$$H = \frac{H_0(6k_1t + 1)}{(k_1t + 1)} \quad (2)$$

Based on eq 2, OA-based crystal growth of anatase TiO_2 NS can be fitted well by the least-squares method and H_0 and k_1 can be calculated as 7.2 nm and 0.22, respectively (see Figure 8). Moreover, the value of H_0 is close to the average thickness of the initial TiO_2 NS.

In addition to the kinetic mechanism, the interfacial integration process was also illustrated to help understanding the crystal growth of anatase TiO_2 NS via elimination of high-energy {001} facets. According to our previous work, the surface of the anatase TiO_2 NS produced with HF as capping agent is covered by F atoms that exist by binding to pentacoordinate Ti atoms on the (001) and (101) surfaces.[10] When the anatase TiO_2 NS were dispersed in deionized water and treated under hydrothermal conditions, Ti−F bonds on the surface would hydrolyze and F atoms can be replaced by hydroxyl (-OH) groups.[49] For this

dx.doi.org/10.1021/cm2008768 |Chem. Mater. 2011, 23, 3486–3494

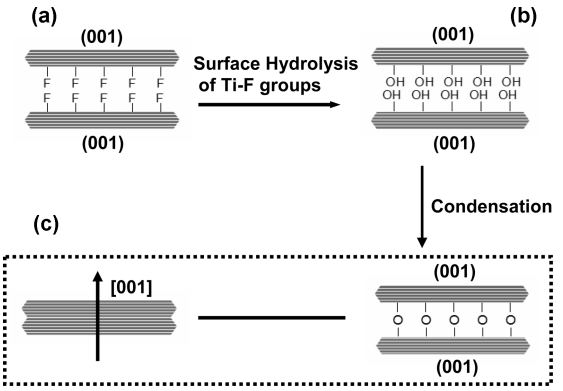

Figure 9. Proposed growth mechanism of stacked anatase TiO_2 nanosheets dominated by {001} facets at their interfacial regions: (a) Stacking of TiO_2 nanosheets with F-terminated surfaces; (b) hydrolysis of Ti−F groups on the surfaces and accordingly the formation of Ti−OH; (c) formation of Ti−O−Ti linkages via condensation between Ti−OH on the (001) surfaces of the adjacent TiO_2 nanosheets and the resulting elimination of (001) surfaces.

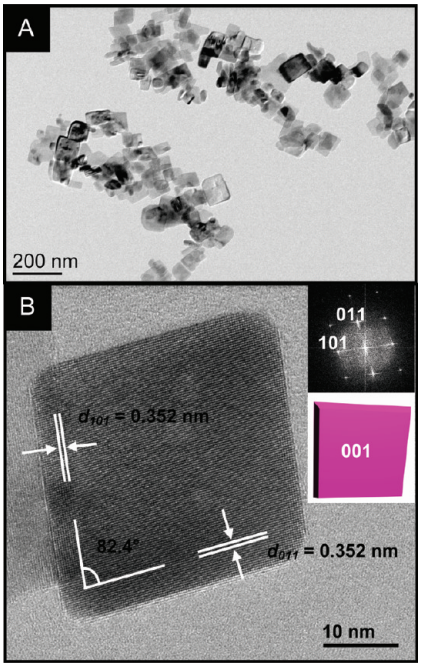

Figure 10. (A) TEM image of the product derived from hydrothermal treatment of anatase TiO_2 nanosheets in HCl aqueous solution (1.5 M) at 200 °C for 88 h. (B) HRTEM image of a typical anatase TiO_2 crystal shown in panel A. (Insets) Corresponding fast Fourier transform (FFT) pattern and schematic model viewed from the $[11\bar{1}]$ direction.

hydrolysis process, the concentration of F^- would increase while the pH value of the aqueous solution decreases gradually as the hydrolysis reaction proceeds continuously. This hydrolytic process can be depicted as

$$\equiv Ti{-}F + H_2O \rightarrow \equiv Ti{-}OH + H^+ + F^- \quad (3)$$

In this case, the exposed surfaces of TiO_2 NS would be mainly covered by -OH groups. Through theoretical predictions,[10] {001} facets have a higher surface energy than {101} facets now. Thus, the exposure of {101} facets become more favorable,

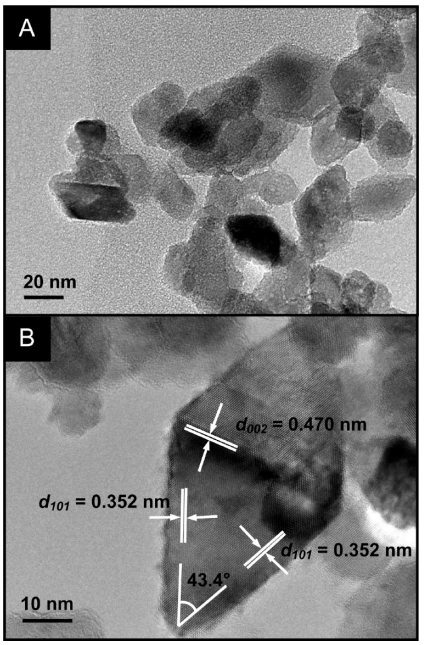

Figure 11. Hydrothermal stability of anatase TiO_2 nanocrystals dominated with {101} facets. (A) Low-magnification TEM image of {101} faceted TiO_2 nanocrystals after hydrothermal treatment in deionized water at 200 °C for 88 h. (B) Corresponding HRTEM image of a single particle.

which can be judged from a Wulff construction model.[6,22] In this work, it can be found that the (001) interfaces between the adjacent anatase TiO_2 NS would be eliminated through the condensation of Ti−OH groups and the Ti−O−Ti linkages can be formed finally. This interfacial crystal growth mechanism of {001} faceted TiO_2 NS via OA process is illustrated in the schematic diagram shown in Figure 9. It should be noted that the surface fusion process is also involved to generate the well-faceted anatase TiO_2 crystals with a flat surface, in which further crystal growth on the surface of the secondary anatase TiO_2 crystals is controlled by diffusion and the initially dissolved TiO_2 in the liquid phase acts as the "nutrient".

Interestingly, it was found that the reaction medium also plays a key role for the OA process of anatase TiO_2 NS under hydrothermal coarsening conditions. Figure 10A shows the low-magnification TEM image of the product prepared by hydrothermal treatment of {001} faceted TiO_2 NS in 1.5 M HCl aqueous solution at 200 °C for 88 h. As judged from the TEM image, the original sheetlike shape was well-maintained, which is quite different from the results with deionized water as reaction medium. Figure 10B present the HRTEM image and the corresponding fast Fourier transform (FFT) pattern of a single free-standing TiO_2 NS. Observed through the $[11\bar{1}]$ zone axis, the HRTEM image in Figure 10B displays (101) and (011) crystal faces with an interfacial angle of 82.4°, which is quite consistent with the theoretical value.[26e] The inset shown in Figure 10B gives the corresponding structural model of the free-standing single crystal. Therefore, the hydrothermal-treated sample is confirmed to be anatase TiO_2 with dominant {001} facets. That is, the morphology of the anatase TiO_2 NS was unchanged after hydrothermal treatment in acidic 1.5 M HCl solution, which has the function to suppress the surface hydrolysis of Ti−F groups and thus block the OA of anatase TiO_2 NS

dx.doi.org/10.1021/cm2008768 |*Chem. Mater.* 2011, 23, 3486–3494

as well. Various alcohols were also utilized as reaction solvents, and the retardation of Ti−F hydrolysis was also found. Figure S4 (Supporting Information) shows TEM images of the samples synthesized by treating anatase TiO_2 NS at 200 °C for 88 h in different alcohol solvents such as ethanol, propanol, and butanol. In this process, it was found that alcohols not only suppress the surface hydrolysis of Ti−F groups but also may help to stabilize the (001) facets as capping agents.[25]

As a further confirmation of the mechanism discussed, anatase TiO_2 nanocrystals dominated by the thermodynamically stable {101} facets[26b] were also hydrothermally treated under the same experimental conditions. As shown in Figure 11A, almost all of the anatase TiO_2 nanocrystals kept their original octahedra morphology well with a particle size of 30−50 nm. The HRTEM image illustrated in Figure 11B provides further structural information, which indicates that the elongated direction of the TiO_2 nanocrystals is parallel to the [001] crystallographic direction, and the interplanar spacing of 0.352 nm and interfacial angle of 43.4° can be assigned to the lattice spacing of adjacent (101) crystal planes and interfacial angle of {101} facets, respectively. All of these observations are basically consistent with the starting {101} faceted anatase TiO_2 reported in the previous work.[26b] Therefore, no significant change occurred in the crystal structure of the anatase TiO_2 nanocrystals with dominant {101} facets after hydrothermal treatment, which confirms the excellent hydrothermal stability of {101} facets of anatase TiO_2.

CONCLUSIONS

In this work, {001} faceted anatase TiO_2 NS were revealed to be unstable during hydrothermal treatment in deionized water. During the treatment, original TiO_2 NS have grown into truncated octahedral TiO_2 via an oriented attachment (OA) process along the [001] crystallographic direction. Under hydrothermal coarsening conditions, hydrolysis of Ti−F groups on the surfaces of TiO_2 NS can induce the combination of adjacent NS in deionized water, which leads to the elimination of high-energetic (001) surfaces. A kinetic model for OA-based crystal growth of {001} faceted anatase TiO_2 NS was proposed and fit well with the experimental results. In addition, reaction media also play an important role in the morphology evolution of anatase TiO_2 NS. In reaction media such as 1.5 M HCl solution, ethanol, propanol, and butanol, the hydrolysis of surface Ti−F can be suppressed effectively and anatase TiO_2 NS can remain their original morphology. The stability study of anatase TiO_2 NS exposed with highly reactive {001} facets would provide an important criterion for their commercial applications and fundamental surface research. The principles found in this work might be applied to other crystalline materials with high-energy facets.

ASSOCIATED CONTENT

Supporting Information. Four figures showing TEM images and XRD spectra of samples with different treatment times, XPS survey spectra of anatase TiO_2 nanosheets before and after hydrothermal reaction, and TEM images of products treated in various solvents. This material is available free of charge via the Internet at http://pubs.acs.org.

AUTHOR INFORMATION

Corresponding Author

*E-mail hgyang@ecust.edu.cn (H.G.Y.); czli@ecust.edu.cn (C.L.).

ACKNOWLEDGMENT

This work was financially supported by Scientific Research Foundation of East China University of Science and Technology (YD0142125), Pujiang Talents Programme and Major Basic Research Programme of Science and Technology Commission of Shanghai Municipality (09PJ1402800, 10JC1403200), Shuguang Talents Programme of Education Commission of Shanghai Municipality (09SG27), National Natural Science Foundation of China (20925621, 20973059, 91022023, 21076076), Fundamental Research Funds for the Central Universities (WJ0913001), and Program for New Century Excellent Talents in University (NCET-09-0347).

REFERENCES

(1) Tian, N.; Zhou, Z. Y.; Sun, S. G.; Ding, Y.; Wang, Z. L. *Science* **2007**, *316*, 732.
(2) Yin, Y.; Alivisatos, A. P. *Nature* **2005**, *437*, 664.
(3) Han, X.; Jin, M.; Xie, S.; Kuang, Q.; Jiang, Z.; Jiang, Y.; Xie, Z.; Zheng, L. *Angew. Chem.* **2009**, *121*, 9344.
(4) Zhang, J.; Langille, M. R.; Personick, M. L.; Zhang, K.; Li, S.; Mirkin, C. A. *J. Am. Chem. Soc.* **2010**, *132*, 14012.
(5) Gong, X. Q.; Selloni, A. *J. Phys. Chem. B* **2005**, *109*, 19560.
(6) Lazzeri, M.; Vittadini, A.; Selloni, A. *Phys. Rev. B* **2001**, *63*, 155409.
(7) Vittadini, A.; Selloni, A.; Rotzinger, F. P.; Grätzel, M. *Phys. Rev. Lett.* **1998**, *81*, 2954.
(8) Diebold, U. *Surf. Sci. Rep.* **2003**, *48*, 53.
(9) Chen, X.; Mao, S. *Chem. Rev.* **2007**, *107*, 2891.
(10) Yang, H. G.; Sun, C. H.; Qiao, S. Z.; Zou, J.; Liu, G.; Smith, S. C.; Cheng, H. M.; Lu, G. Q. *Nature* **2008**, *453*, 638.
(11) Chen, X.; Shen, S.; Guo, L.; Mao, S. *Chem. Rev.* **2010**, *110*, 6503.
(12) O'Regan, B.; Grätzel, M. *Nature* **1991**, *353*, 737.
(13) Grätzel, M. *Nature* **2001**, *414*, 338.
(14) Barbé, C. J.; Arendse, F.; Comte, P.; Jirousek, M.; Lenzmann, F.; Shklover, V.; Grätzel, M. *J. Am. Ceram. Soc.* **1997**, *80*, 3157.
(15) Snaith, H. J.; Schmidt-Mende, L. *Adv. Mater.* **2007**, *19*, 3187.
(16) Fujishima, A.; Honda, K. *Nature* **1972**, *238*, 37.
(17) Varghese, O. K.; Paulose, M.; LaTempa, T. J.; Grimes, C. A. *Nano Lett.* **2009**, *9*, 731.
(18) Lazzeri, M.; Selloni, A. *Phys. Rev. Lett.* **2001**, *87*, 266105.
(19) Penn, R. L.; Banfield, J. F. *Geochim. Cosmochim. Acta* **1999**, *63*, 1549.
(20) Zaban, A.; Aruna, S. T.; Tirosh, S.; Gregg, B. A.; Mastai, Y. *J. Phys. Chem. B* **2000**, *104*, 4130.
(21) Jun, Y. W.; Casula, M. F.; Sim, J. H.; Kim, S. Y.; Cheon, J.; Alivisatos, A. P. *J. Am. Chem. Soc.* **2003**, *125*, 15981.
(22) Barnard, A. S.; Curtiss, L. A. *Nano Lett.* **2005**, *5*, 1261.
(23) Yang, H. G.; Zeng, H. C. *J. Phys. Chem. B* **2004**, *108*, 3492.
(24) Yang, H. G.; Zeng, H. C. *J. Am. Chem. Soc.* **2005**, *127*, 270.
(25) Yang, H. G.; Liu, G.; Qiao, S. Z.; Sun, C. H.; Jin, Y.; Smith, S. C.; Zou, J.; Cheng, H. M.; Lu, G. Q. *J. Am. Chem. Soc.* **2009**, *131*, 4078.
(26) (a) Ma, X. Y.; Chen, Z. G.; Hartono, S. B.; Jiang, H. B.; Zou, J.; Qiao, S. Z.; Yang, H. G. *Chem. Commun.* **2010**, *46*, 6608. (b) Sun, C. H.; Yang, X. H.; Chen, J. S.; Li, Z.; Lou, X. W.; Li, C.; Smith, S. C.; Lu, G. Q.; Yang, H. G. *Chem. Commun.* **2010**, *46*, 6129. (c) Yang, X. H.; Li, Z.; Liu, G.; Xing, J.; Sun, C. H.; Yang, H. G.; Li, C. Z. *CrystEngComm* **2011**, *13*, 1378. (d) Fang, W. Q.; Zhou, J. Z.; Liu, J.; Chen, Z. G.; Yang, C.; Sun, C. H.; Qiao, G. R.; Zou, J.; Qiao, S. Z.; Yang, H. G. *Chem.—Eur. J.* **2011**, *17*, 1423–1427. (e) Zhu, J.; Wang, S.; Bian, Z.; Xie, S.; Cai, C.; Wang, J.; Yang, H. G.; Li, H. X. *CrystEngComm* **2010**, *12*, 2219.
(27) (a) Liu, G.; Yang, H. G.; Wang, X.; Cheng, L.; Pan, J.; Lu, G. Q.; Cheng, H. M. *J. Am. Chem. Soc.* **2009**, *131*, 12868. (b) Liu, G.; Sun, C. H.; Yang, H. G.; Smith, S. C.; Wang, L. Z.; Lu, G. Q.; Cheng, H. M. *Chem. Commun.* **2010**, *46*, 755. (c) Liu, G.; Yang, H. G.; Wang, X.; Cheng, L.; Lu, H.; Wang, L.; Lu, G. Q.; Cheng, H. M. *J. Phys. Chem. C* **2009**, *113*, 21784.

(28) (a) Han, X.; Kuang, Q.; Jin, M.; Xie, Z.; Zheng, L. *J. Am. Chem. Soc.* **2009**, *131*, 3152. (b) Wu, B. H.; Guo, C. Y.; Zheng, N. F.; Xie, Z. X.; Stucky, G. D. *J. Am. Chem. Soc.* **2008**, *130*, 17563.
(29) (a) Dai, Y. Q.; Cobley, C. M.; Zeng, J.; Sun, Y. M.; Xia, Y. N. *Nano Lett.* **2009**, *9*, 2455. (b) Zheng, Z.; Huang, B.; Qin, X.; Zhang, X.; Dai, Y.; Jiang, M.; Wang, P.; Whangbo, M. H. *Chem.—Eur. J.* **2009**, *15*, 12576.
(30) (a) Yu, J.; Xiang, Q.; Ran, J.; Mann, S. *CrystEngComm* **2010**, *12*, 872. (b) Liu, S.; Yu, J.; Jaroniec, M. *J. Am. Chem. Soc.* **2010**, *132*, 11914. (c) Yu, J.; Qi, L.; Jaroniec, M. *J. Phys. Chem. C* **2010**, *114*, 13118. (d) Xiang, Q.; Lv, K.; Yu, J. *Appl. Catal. B: Environ.* **2010**, *96*, 557.
(31) (a) Chen, J. S.; Tan, Y. L.; Li, C. M.; Cheah, Y. L.; Luan, D. Y.; Madhavi, S.; Boey, F. Y. C.; Archer, L. A.; Lou, X. W. *J. Am. Chem. Soc.* **2010**, *132*, 6124. (b) Chen, J. S.; Lou, X. W. *Electrochem. Commun.* **2009**, *11*, 2332.
(32) (a) Zhang, D.; Li, G.; Yang, X.; Yu, J. C. *Chem. Commun.* **2009**, *29*, 4381. (b) Zhang, D.; Li, G.; Wang, H.; Chan, K. M.; Yu, J. C. *Cryst. Growth Des.* **2010**, *10*, 1130.
(33) (a) Liu, M.; Piao, L.; Zhao, L.; Ju, S.; Yan, Z.; He, T.; Zhou, C.; Wang, W. *Chem. Commun.* **2010**, *46*, 1664. (b) Liu, M.; Piao, L.; Lu, W.; Ju, S.; Zhao, L.; Zhou, C.; Li, H.; Wang, W. *Nanoscale* **2010**, *2*, 1115.
(34) (a) Alivov, Y.; Fan, Z. Y. *J. Phys. Chem. C* **2009**, *113*, 12954. (b) Li, J.; Yu, Y.; Chen, Q.; Li, J.; Xu, D. *Cryst. Growth Des.* **2010**, *10*, 2111. (c) Amano, F.; Prieto-Mahaney, O. O.; Terada, Y.; Yasumoto, T.; Shibayama, T.; Ohtani, B. *Chem. Mater.* **2009**, *21*, 2601. (d) Hu, X.; Zhang, T.; Jin, Z.; Huang, S.; Fang, M.; Wu, Y.; Zhang, L. D. *Cryst. Growth Des.* **2009**, *9*, 2324.
(35) Selloni, A. *Nat. Mater.* **2008**, *7*, 613.
(36) Herman, G. S.; Sievers, M. R.; Gao, Y. *Phys. Rev. Lett.* **2000**, *84*, 3354.
(37) Hengerer, R.; Bolliger, B.; Erbudak, M.; Grätzel, M. *Surf. Sci.* **2000**, *460*, 162.
(38) (a) Penn, R. L.; Banfield, J. F. *Science* **1998**, *281*, 969. (b) Penn, R. L.; Banfield, J. F. *Am. Mineral.* **1998**, *83*, 1077. (c) Zhang, H.; Banfield, J. F. *Am. Mineral.* **1999**, *84*, 528. (d) Finnegan, M. P.; Zhang, H.; Banfield, J. F. *J. Phys. Chem. C* **2007**, *111*, 1962. (e) Finnegan, M. P.; Zhang, H.; Banfield, J. F. *Chem. Mater.* **2008**, *20*, 3443.
(39) (a) Zhang, J.; Huang, F.; Lin, Z. *Nanoscale* **2010**, *2*, 18. (b) Zhuang, Z.; Zhang, J.; Huang, F.; Wang, Y.; Lin, Z. *Phys. Chem. Chem. Phys.* **2009**, *11*, 8516. (c) Xiong, Y.; Zhang, J.; Huang, F.; Ren, G.; Liu, W.; Li, D.; Wang, C.; Lin, Z. *J. Phys. Chem. C* **2008**, *112*, 9229. (d) Zhang, J.; Lin, Z.; Lan, Y.; Ren, G.; Chen, D.; Huang, F.; Hong, M. *J. Am. Chem. Soc.* **2006**, *128*, 12981.
(40) (a) Zeng, H. C. *Int. J. Nanotechnol.* **2007**, *4*, 329. (b) Chen, J. S.; Zhu, T.; Li, C. M.; Lou, X. W. *Angew. Chem., Int. Ed.* **2011**, *50*, 650.
(41) Zhang, Q.; Liu, S.; Yu, S. *J. Mater. Chem.* **2009**, *19*, 191.
(42) Delley, B. *J. Chem. Phys.* **1990**, *92*, 508.
(43) Delley, B. *J. Chem. Phys.* **2000**, *113*, 7756.
(44) Perdew, J. P.; Burke, K.; Ernzerhof, M. *Phys. Rev. Lett.* **1996**, *77*, 3865.
(45) Schliehe, C.; Juarez, B. H.; Pelletier, M.; Jander, S.; Greshnykh, D.; Nagel, M.; Meyer, A.; Foerster, S.; Kornowski, A.; Klinke, C.; Weller, H. *Science* **2010**, *329*, 550.
(46) Yu, J. C.; Yu, J.; Ho, W.; Jiang, Z.; Zhang, L. *Chem. Mater.* **2002**, *14*, 3808.
(47) Huang, F.; Zhang, H.; Banfield, J. F. *J. Phys. Chem. B* **2003**, *107*, 10470.
(48) Huang, F.; Zhang, H.; Banfield, J. F. *Nano Lett.* **2003**, *3*, 327.
(49) Yang, H. G.; Zeng, H. C. *J. Phys. Chem. B* **2003**, *107*, 12244.